Stacking faults in 3*C*-, 4*H*-, and 6*H*-SiC polytypes investigated by an *ab initio* supercell method

Ulf Lindefelt,[1,2,3] Hisaomi Iwata,[1,2] Sven Öberg,[4] and Patrick R. Briddon[5]
[1]*Department of Physics and Measurement Technology, Linköping University, SE-581 83 Linköping, Sweden*
[2]*Department of Microelectronics and Information Technology, Royal Institute of Technology (KTH), Electrum 229, SE-164 40 Kista, Sweden*
[3]*ABB Group Services Center, Corporate Research, SE-721 78 Västerås, Sweden*
[4]*Department of Mathematics, Luleå University of Technology, SE-971 87 Luleå, Sweden*
[5]*Department of Physics, University of Newcastle upon Tyne, Newcastle NE1 7RU, United Kingdom*
(Received 29 June 2002; revised manuscript received 13 November 2002; published 9 April 2003)

Recent attempts to make SiC diodes have revealed a problem with stacking fault expansion in the material, leading to unstable devices. In this paper, we present detailed results from a density-functional supercell calculation on the electronic structure of stacking faults which result from glide of Shockley partials in 3*C*-, 4*H*- and 6*H*-SiC. It was found [Phys. Rev. B **65**, 033203 (2002)] that both types of stacking faults in 4*H*-SiC and two types of stacking faults in 6*H*-SiC give rise to band states, which are strongly localized (confined within around 10 Å) in the direction orthogonal to the stacking fault plane. Based on estimates of the band offsets between different polytypes and a simple quantum-well theory, we show that it is possible to interpret this one-dimensional localization as a quantum-well confinement effect. We also find that the third type of stacking fault in 6*H*-SiC and the only stacking fault in 3*C*-SiC do not give rise to states clearly separated from the band edges, but instead give rise to rather strongly localized band states with energies very close to the band edges. We argue that these localized near band edge states are created by stacking fault induced changes in the dipole moment associated with the hexagonal symmetry. In addition, we have also calculated the stacking fault energies, using both the supercell method and the simpler ANNNI (axial next nearest-neighbor Ising) model. Both theories agree well with the low stacking fault energies found experimentally.

DOI: 10.1103/PhysRevB.67.155204 PACS number(s): 71.23.An, 71.15.−m

I. INTRODUCTION

For many years, SiC has been praised for its outstanding material properties and considered the most advantageous near-future choice of material for making power electronic devices, possibly to be superseded only by diamond. Recently, however, it was discovered[1–3] that the material suffers from an unexpected weakness: diodes manufactured from 4*H*-SiC gradually degraded in the sense that the voltage drop across the diode, for a constant current, gradually increased with the time of operation. The increase in voltage drop, compared to its ideal value (typically around 3.4 V at a current density of 100 A/cm^2) was typically in the range from several mV to several tenths of a V, even up to more than 1 V in some cases. Since the area of present days diodes are limited to approximately 1 cm^2, many real applications require parallel coupling of diodes, with the consequence that stochastic degradation even in the mV range becomes problematic.

In two recent brief articles[4] we argued that this type of diode degradation was caused by the propagation of partial dislocations, resulting in the creation of stacking faults (SF's) penetrating the active region of the device. The argument was based on our discovery that SF's in the (0001) glide plane, even though they are not associated with broken or dangling bonds, give rise to states which are bound in the sense that they are strongly localized in the direction perpendicular to the SF plane, and have an energy around 0.2 eV below the lowest conduction band. A similar conclusion was recently also arrived at by Miao *et al.*[5] Electrons which are trapped in such states are thus hindered in their motion along the main electron-drift direction, which typically (for growth reasons) forms an angle 8° relative to the [0001] direction. The electrons are, however, free to move along the SF plane. This picture seems to be fully consistent with later experimental work around the causes for degradation in SiC diodes.[6,7] It is therefore felt that increased knowledge and understanding of SF's in this material are of importance.

In this paper we shall give a more detailed account of the work leading to the results summarized in Ref. 4. We will thus consider the effects of SF's in the three polytypes 3*C*-, 4*H*-, and 6*H*-SiC in considerably more detail. In addition, we will also present our results on the calculation of SF energies in these polytypes, i.e., the cost in energy to produce a SF in a (0001) plane. The SF energies have been calculated using both an *ab initio* supercell method and the simpler, semianalytical ANNNI (axial next-nearest-neighbor Ising) model.[8,9] It will be seen that both methods agree well with experimentally determined values of the SF energies.

II. STRUCTURAL MODELS

A. Stacking faults produced by partial dislocation glide

Extended SF regions can be created by the motion of partial dislocations, leaving behind a faulted crystal containing an error in the stacking sequence (i.e., a SF). In this paper, as well as in Refs. 4 and 5, attention is confined to dislocations from the *glide set*, which are generally consid-

0163-1829/2003/67(15)/155204(12)/$20.00 ©2003 The American Physical Society

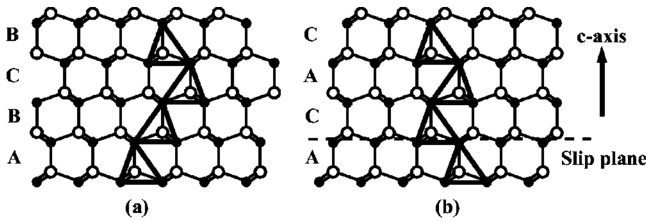

FIG. 1. Tetrahedral stacking sequence, viewed from a $[11\bar{2}0]$ direction, of $4H$-SiC (a) before and (b) after the passage of a leading partial dislocation. Open (filled) circles denote Si (C) atoms and the dashed horizontal line represents the slip plane. The atomic positions in the various layers are indicated using the classical ABC notation. In (a) the two tetrahedra in the middle are called "normal," whereas the other two are called "twinned." A partial dislocation from the glide set transforms a normal (twinned) tetrahedron into a twinned (normal) tetrahedron, which can take place in any slip plane. A partial from the shuffle set (not considered here) corresponds to a slip in the plane between the Si and C atoms bonded along the c direction.

ered much more likely than dislocations from the shuffle set (cf. Fig. 1). In the hexagonal SiC polytypes, the partial dislocations can move by glide in the (0001) basal plane [corresponding to the (111) glide plane for the cubic polytype $3C$-SiC]. For instance, a complete dislocation with the Burgers vector $a/3\langle 2\overline{1}\overline{1}0\rangle$, where a is the lattice constant in the basal plane, can dissociate into two partial dislocations according to the Burgers vector reaction formula[9–11]

$$a/3\langle 2\overline{1}\overline{1}0\rangle \rightarrow a/3\langle 1\overline{1}00\rangle + a/3\langle 10\overline{1}0\rangle. \tag{1}$$

Each partial corresponds to a slip of the upper part of the crystal relative to the lower part by a nonprimitive translation vector, thus creating a SF on the back side of its direction of propagation. An example of a SF in $4H$-SiC is illustrated in Fig. 1, which shows the atomic positions in a perfect and in a faulted crystal, projected onto a $(11\bar{2}0)$ plane. Using the classical ABC notation, the stacking sequence of perfect $4H$-SiC is $\cdots$(ABCB)(ABCB)(ABCB)$\cdots$. One of the partials in Eq. (1) induces a change A→B, B→C, and C→A (referred to as partial L), and the other partial induces the change A→C, B→A, and C→B (referred to as partial R). The propagation of partial L between layers A and B in a unit cell of $4H$-SiC gives the faulted sequence $\cdots$(ABCB)(A|CAC)(BCAC)$\cdots$, where | denotes the slip plane. This is the case illustrated in Fig. 1(b). Note that partial R cannot propagate through this plane of the perfect crystal, since that would violate the hexagonal stacking sequence (which does not permit an A plane on an A plane, etc.). As another possibility, partial L can also propagate between layers B and C in $4H$-SiC, giving the faulted sequence $\cdots$(ABCB)(AB|AC)(BCAC)$\cdots$. We will refer to these two faulted sequences in $4H$-SiC as SF I and SF II, respectively.

When dealing with SF's, the classical ABC notation, which in a sense refers to the absolute positions of atomic layers, is rather clumsy. It is usually more transparent to use the Hägg notation, and the related Zhdanov notation, which both refer to the relative positions of layers. In the Hägg notation, the stacking orders AB, BC, and CA are all denoted (+), whereas the reverse stacking orders BA, CB, and AC are all denoted (−). With this notation, $3C$-, $4H$-, and $6H$-SiC can be represented as a repetition of (+++), (++−−), and (+++−−−) unit cells, respectively. The Zhdanov symbols consist of pairs of numbers in which the first number denotes the number of consecutive plus signs, and the second the number of consecutive minus signs (if at all appearing). With the Zhdanov notation, these three polytypes are denoted (3), (22), and (33), respectively, referring to a single unit cell. With the notation (22)*, for instance, we refer to a stacking sequence (−−++) starting with a minus sign, which is obtained form (22) by a 180° rotation around the hexagonal c axis.

Partial L (R) changes a plus (minus) sign in the Hägg sequence immediately above the glide plane to a minus (plus) sign, leaving all the other signs in the Hägg sequence unaltered. Thus, SF I in $4H$-SiC corresponds to (−+−−), or (122)* in the faulted cell [see Fig. 1(b)], and SF II corresponds to (+−−−), or (13). We can tentatively denoted these SF's as SF(112)* (same as SF I) and SF(13) (same as SF II).

Now, sending partial R through the plane between C and B in the perfect $4H$-SiC crystal (ABC|B) produces the Hägg sequence $\cdots$(++−−)(+++−)(++−−)$\cdots$, which corresponds to (31) in the faulted cell. However, this sequence can be obtained from SF(112)* in $4H$-SiC, i.e., from (++−−)(−+−−)(++−−), by first performing a 180° rotation around the c axis [producing (−−++)(+−++)(−−++)], followed by a translation c/2 along the hexagonal c axis, formally corresponding to moving the parentheses two steps to the left. (Note that this symmetry operation is contained in the nonsymmorphic space group C_{6v}^4 for $4H$- and $6H$-SiC.) Thus, instead of using the notation SF(112)* we can as well use the notation SF(31) to denote SF I. The argument for the remaining glide plane is similar, leading to SF II, i.e., SF(211)=SF(13), in $4H$-SiC. To summarize, in $4H$-SiC, SF I is equivalent to SF(31), and SF II is equivalent to SF(13). We will use these different notations for SF's interchangeably.

In $3C$-SiC there is of course only one type of SF that can be introduced by dislocation glide. It can be denoted SF(111). Using the same arguments as above, we find that there are three types of SF's in $6H$-SiC: SF I, defined as (A|CABAC) inside the faulted cell, which can be denoted SF(42), SF II, defined as (AB|ABAC), which can be denoted SF(3111) [or SF(1113)], and SF III, defined as (ABC|BAC), which can be denoted SF(24).[12] The different cases are illustrated in Fig. 2. We can find no operations from the space group C_{6v}^4 which transform a $4H$-SiC crystal containing SF(31) into a crystal containing SF(13), or which transform SF(42) in $6H$-SiC into SF(24). We therefore conclude that there are two types of nonequivalent SF's that can be introduced by glide in $4H$-SiC, and three types of nonequivalent SF's in $6H$-SiC.

It should be noted that SF(31) and SF(13) in $4H$-SiC and SF(42) and SF(24) in $6H$-SiC are related through an interchange of Si and C atoms (plus a 180° rotation around an axis perpendicular to the hexagonal c axis). In contrast to the perfect crystal, such an interchange of atoms does not leave

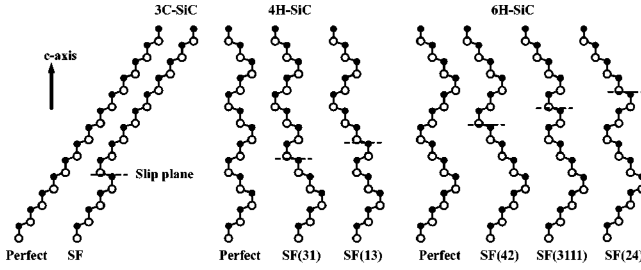

FIG. 2. Geometrically distinguishable SF's obtained by glide in 3*C*- and 6*H*-SiC in different glide planes (dashed horizontal lines), viewed from a $[11\bar{2}0]$ direction. Associating the Hägg sequence signs + and − with steps to the right and left, respectively, the stacking sequence shown in the case SF(31) [SF(42), SF(3111)] is actually that for the equivalent case SF(112)* [SF(123)*, SF(1113)]. SF(31) [SF(42)] and SF(13) [SF(24)] in 4*H*-[6-*H*-] SiC are related through an interchange of Si and C atoms.

the Hamiltonian for the faulted crystal invariant, in the same way as the Hamiltonian for a crystal containing a point defect is not invariant under such an operation (which transforms, for instance, a Si vacancy into SiC into a C vacancy). We also note that the number of different types of SF's introduced by glide in various polytypes apparently coincides with the number of different energy levels associated with a given defect state. For instance, it is well known that substitutional N in SiC gives rise to one, two, and three different donor levels in 3*C*-, 4*H*-, and 6*H*-SiC, respectively, corresponding to the different planes in which the N atom is present.

Since SF(31) and SF(13) in 4*H*-SiC (and correspondingly in 6*H*-SiC) are related through an interchange of Si and C atoms, the notations used so far do not uniquely specify the geometrical structure of the SF before the relative positions of the Si and C atoms are specified. Here we will use the convention that each bilayer consists of a C atom on "top" of a Si atom, i.e., a vector from the Si atom to its partner C atom in the bilayer is in the *positive c* direction ("up"), as in Fig. 1. Furthermore, the notation SF(31) etc. has the advantage over the notation SF I, etc., that the sum of the integers in the Zhdanov notation automatically also specifies the polytype, i.e., the former notation specifies both the polytype and the particular SF under consideration.

B. Models for stacking fault energy

The SF energy γ is defined as $\gamma=[E(\text{faulted})-E(\text{perfect})]/A$, where A is the interface area, E(faulted) is the total energy of the crystal with a SF, and E(perfect) is the total energy of the perfect crystal. As will be described below, the present investigation applies a supercell approach to calculate energies and wave functions, in which case the total energies refer to the total energy of a supercell, and the area $A=a^2\sqrt{3}/2$ is the area of the supercell in the (0001) basal plane.

For many SiC polytypes, the SF energy is found to be small, in some cases a few mJ/m^2,[9,10] i.e., a few meV per atomic pair. Applying the *ab initio* method to supercells containing several tens or up to around 100 atoms, one may have legitimate doubts about the accuracy of the difference between total energies per supercell to deduce such small SF energies. To monitor the accuracy to some extent at least, we have therefore also calculated the SF energies using the ANNNI model. In this model,[8,9] the SF energies can be expressed as (with the subscripts on γ denoting polytype and type of SF, respectively)

$$\begin{aligned}\gamma_{3C}&=4\cdot(J_1+J_2+J_3)/A,\\ \gamma_{4H,\mathrm{I}}&=\gamma_{4H,\mathrm{II}}=-4J_2/A,\\ \gamma_{6H,\mathrm{I}}&=\gamma_{6H,\mathrm{III}}=-4J_3/A,\\ \gamma_{6H,\mathrm{II}}&=4\cdot(J_1-J_2-J_3)/A,\end{aligned}\tag{2}$$

where the J parameter can be obtained in terms of the total energies E_{3C}, E_{2H}, E_{4H}, and E_{6H} per Si-C pair in the perfect crystal using much smaller unit cells:

$$\begin{aligned}J_1&=(2E_{2H}-E_{3C}+3E_{4H}-3E_{6H})/4,\\ J_2&=-(E_{2H}+E_{3C}-2E_{4H})/4,\\ J_3&=-(E_{3C}+2E_{4H}-3E_{6H})/4.\end{aligned}\tag{3}$$

We note that according to the ANNNI model, SF(31) and SF(13) in 4*H*-SiC, as well as SF(42) and SF(24) in 6*H*-SiC, have the same SF energies. We will see later that this is a property of the ANNI model and only approximately true.

III. THE *ab initio* SUPERCELL MODEL

The (Kohn–Sham) band structure and total energies of supercells are calculated using a method based on the self-consistent density functional theory. Only a brief summary of the main points is given here; for a more detailed description see Ref. 13. A basis set of Gaussian orbitals is used to describe the Kohn–Sham wave functions. Suitable multiplicative factors provide *s*- and *p*-, and optionally for each exponent, *d*-orbital symmetries. In order to establish a reasonable balance between speed and reliability for the calculations, several pseudopotentials and many basis sets were constructed, and tested. Both norm-conserving pseudopotentials based on the Troullier-Martins scheme[14] and the Bachelet-Hamann-Schlüter scheme[15] were used. The latter pseudopotentials were used in the present calculations with the spin-averaged local-density approximation. The charge density is represented by a plane-wave basis in reciprocal space. An automatic procedure ensures that the number of shells of real-space lattice vectors used to evaluate the Madelung energy is sufficient. We use the Monkhorst-Pack (MP) scheme[16] to sample the band structure. Both the largest reciprocal lattice vectors of the charge-density Fourier expansion, and the mesh of **k** points are chosen so that the total energy is converged with respect to these parameters. Proper account is taken of the band structure for the occupancies of each Kohn–Sham level. The states are filled according to a Fermi function with a small, finite temperature that is chosen to improve the numerical stability of the self-consistency procedure. A correction is applied to the total energy to account for the entropy that this introduces. The forces acting

TABLE I. Values of calculated and experimental hexagonal lattice constants a (basal plane) and c (orthogonal to the basal plane) in Å. The value of c is presented after division by (na), where n is the number of bilayers in the unit cell, i.e., n=3, 4, and 6 for $3C$-, $4H$- and $6H$-SiC, respectively.

Lattice constant (Å)		$3C$-SiC	$4H$-SiC	$6H$-SiC
a	Theory (present)	3.049	3.044	3.045
	Exp. (Ref. 17)	3.082	3.073	3.080
	Exp. (Ref. 18)		3.08051	3.08129
$c/(\mathrm{n}a)$	Theory (present)	0.81650	0.81947	0.81886
	Exp. (Ref. 17)	0.81650	0.81785	0.81804
	Exp. (Ref. 18)		0.81844	0.81781

on each atom are given by an analytical formula derived from the total energy expression. Structural optimization to minimize the total energy is performed by a conjugate-gradient algorithm. The method is thus a state-of-the-art local-density method. We have made no attempts to correct the value of the Kohn–Sham band gap, which will thus be smaller than the true fundamental band gap.

To model the effects of SF's in the (0001) glide planes we are using supercells which coincide with the primitive unit cells in the (0001) plane, but which are elongated relative to the primary unit cell along the c direction. By choosing the elongation in the c direction sufficiently large, we can avoid SF-SF interactions. One must note, however, that since the SF contained in the supercell corresponds to a nonprimitive translation in the basal plane [see Eq. (1)] by a part of the supercell, translational symmetry in all three dimensions requires that we tilt the c axis to an amount and direction given by the Burgers vector corresponding to the partial dislocation imagined to have produced the SF. This gives rise to a rhombohedral (triclinic) supercell, whose lattice constant c' in the tilted c direction has the projected length c along the hexagonal c axis.

When viewed as a hexagonal structure, $3C$-SiC has 6 atoms in the primitive unit cell, whereas $4H$- and $6H$-SiC have 8 and 12 atoms per primitive cell, respectively. In order to determine the perfect crystal *ab initio* lattice constants (by total energy minimization), the perfect crystal atomic positions (by intrasupercell atomic relaxation) and the J parameters in the ANNNI model, we have employed supercells containing 24 atoms for all these polytypes, i.e., the supercells for $3C$-, $4H$-, and $6H$-SiC consist of 4, 3, and 2 primitive unit cells stacked on top of one another, respectively. Our reason for not choosing the smallest possible unit cell in each case, but rather unit cells containing the same number of atoms for the three cases, is that it is preferable to employ the same size of the supercell for all polytypes, since cancellation of systematic errors are then expected to some extent when the total energies of different polytypes are compared.

In all cases where SF's have been studied, we have used rhombohedral supercells containing 96 atoms, i.e., containing, 16, 12, and 8 primitive unit cells for $3C$-, $4H$-, and $6H$-SiC, respectively, stacked on top of one another, making the artificial SF-SF interaction negligible. Intrasupercell

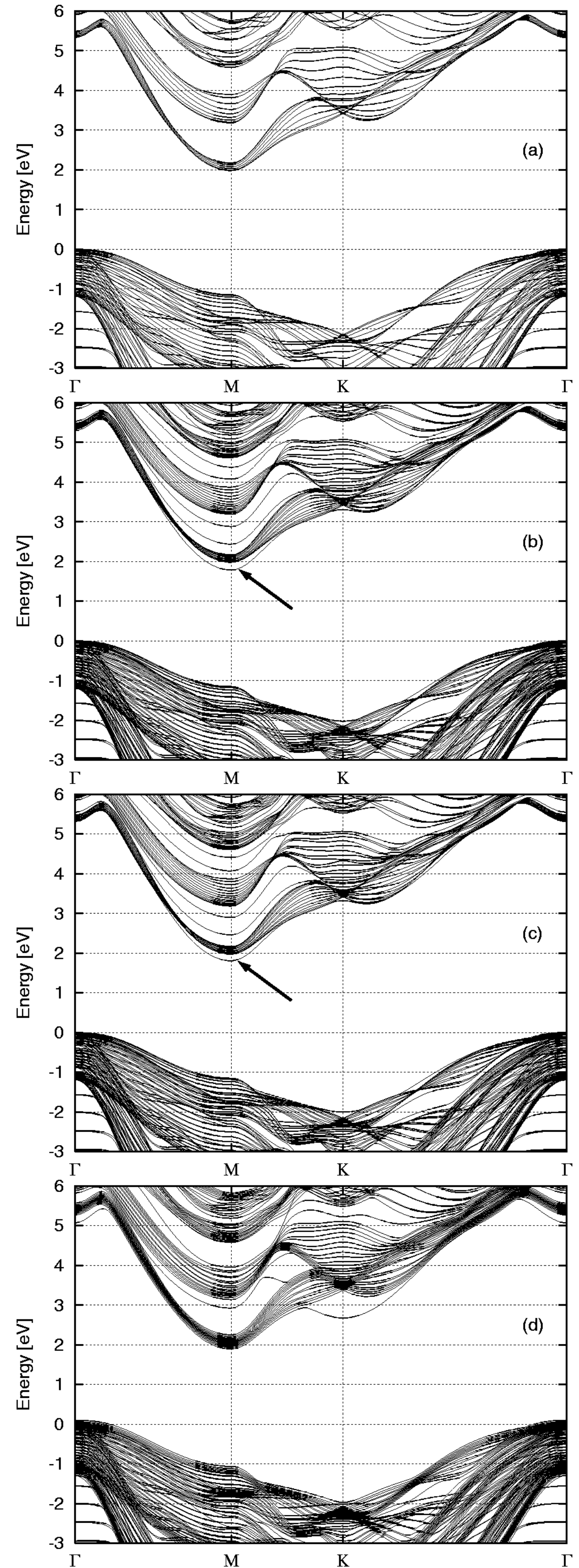

FIG. 3. Kohn-Sham band structure for 96 atom supercells for (a) perfect $6H$-SiC, (b) with SF(42), (c) with SF(24), and (d) with SF(3111). The arrows point at the split-off bands below the conduction band caused by the SF.

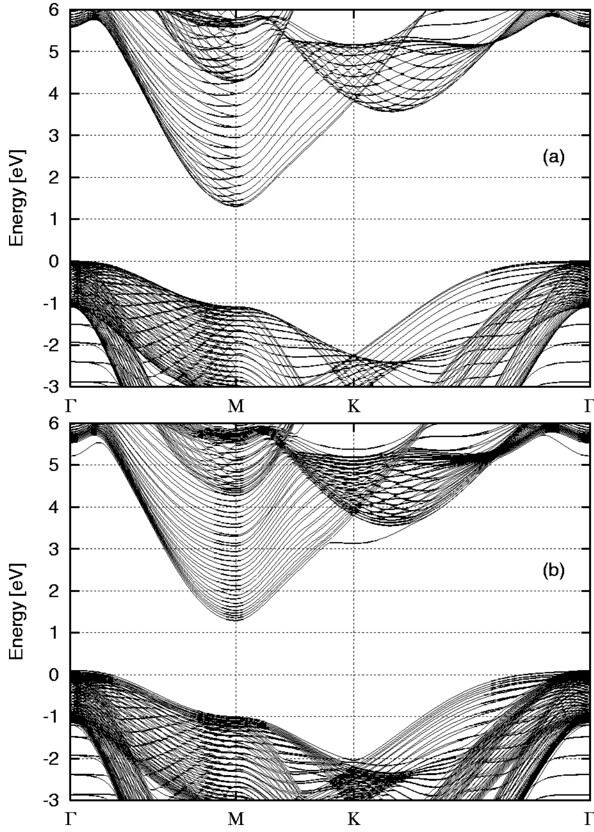

FIG. 4. Kohn-Sham band structure for 96 atom supercells for (a) perfect 3C-SiC and (b) with SF(111).

atomic relaxations have also been performed in the presence of SF's by requiring the vanishing of the Hellmann-Feynman force on each atom. It was found that such relaxations have very little influence on the bandstructure, but affect the SF energies to some extent.

Since the supercells are extended along the c direction, the Brillouin zone is practically two dimensional. All Brillouin zone interactions have been replaced by summations over six special MP **k** points[16] in the basal plane of the Brillouin zone.

As a simple and partial illustration of the accuracy of the computational method, we compare in Table I experimental lattice parameters of the perfect crystals with those obtained with the present method. The theoretical results are in good agreement with the experimental results.

IV. THE ELECTRONIC STRUCTURE OF STACKING FAULTS

A. The quantum-well confinement of the stacking-fault gap states

In Ref. 4 we displayed the 96 atom supercell band structure for 4H-SiC with and without SF(31) along the closed path Γ-M-K-Γ in the Brillouin zone. The band structure for SF(13) turns out to be very similar to that for SF(31). In Fig. 3 we show the corresponding band structures for SF(42), SF(24), and SF(3111) in 6H-SiC, and in Fig. 4 for SF(111) in 3C-SiC. The important features are (1) the existence of clearly split-off bands below the conduction band in the cases SF(31), SF(13), SF(42), and SF(24), (2) no clearly split-off bands below the conduction bands in the cases SF(3111) and SF(111), and (3) no clear effect at the top of the valence bands in any of the cases. The split-off energies, i.e., the energy difference between the minimum of the (modified) conduction band and the minimum of the split-off band, were presented in Ref. 4, but are reproduced in Table II for convenience, together with other new information that will be used in the discussion below.

In order to reveal more about the nature of the split-off band below the bottom of the conduction band, we will study the wave functions corresponding to various states. To reduce the amount of data, without loosing too much relevant information, we have chosen to plot the function[4]

$$f_{\alpha}(z)=\int\int|\Psi_{\alpha}(x,y,z)|^{2}dxdy, \qquad (4)$$

where α denotes a **k** point in the Brillouin zone (e.g., $\alpha=\Gamma$ or M), Ψ_{α} is the wave function for a certain state (band) at this **k** point, and the integration for each value of z along the (tilted) c axis is performed in the basal plane within the supercell. One can think of $f_{\alpha}(z)$ as the probability to find an electron in the given state at a particular value of z away

TABLE II. Electronic structure data for different SF's in three SiC polytypes. E_B is the energy of the split-off band minimum below the conduction band minimum, with ~0 indicating cases where no clearly split-off states are seen, w_B, w_C, and w_V are the localization parameters [w, defined below Eq. (5)] for the minimum of the split-off band, for the localized band state just below the bottom of the extended band state at the conduction band minimum, and for the localized band state just above the top of the extended band state at the valence band maximum, respectively. $E_{B,\mathrm{QW}}$ and $w_{B,\mathrm{QW}}$ are the energy and wave function localization parameter obtained using the simple QW model described in the main text.

Polytype	Type of SF	E_B [eV]	w_B [Å]	$E_{B,\mathrm{QW}}$ [eV]	$w_{B,\mathrm{QW}}$ [Å]	w_C/w_V [Å]
3C	SF(111)	~0				30/18
4H	SF(31)	−0.22	7.2	−0.24	6.1	
	SF(13)	−0.18	8.6	−0.24	6.1	/28
6H	SF(42)	−0.19	8.0	−0.22	6.5	
	SF(3111)	~0				15/15
	SF(24)	−0.17	9.5	−0.22	6.5	/42

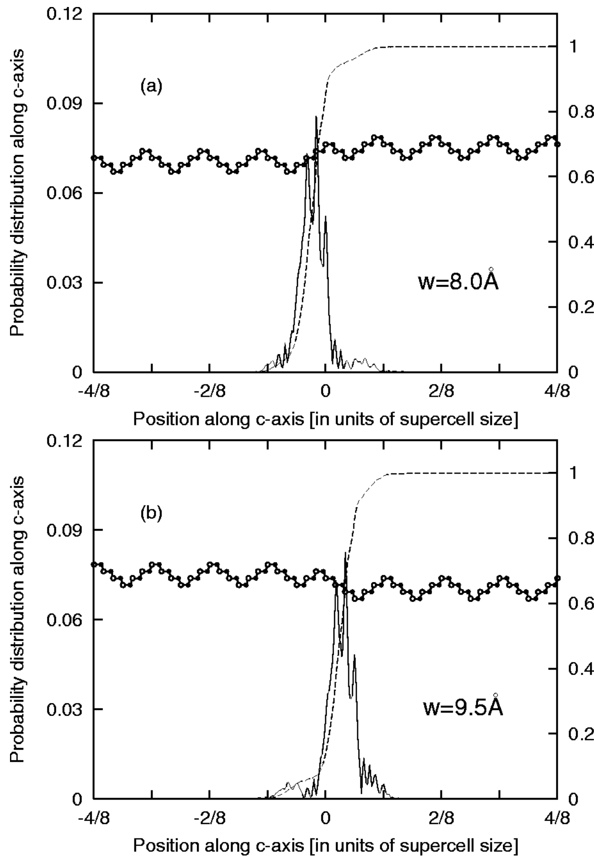

FIG. 5. The projected probability distribution [Eq. (4)] (left-hand scale) and the truncated normalization integral [Eq. (5)] (right-hand scale), within a 96 atom supercell, for the split-off band at M in the case (a) SF(42) and (b) SF(24) in $6H$-SiC. Also shown are the stacking sequence and the localization (w).

from the SF plane. Alternatively, it describes the projection of the three-dimensional probability distribution onto and along the c axis. As a further illustration of the degree of localization, we also consider the truncated normalization integral

$$I_{\alpha}(z)=\int^{z} f_{\alpha}(z')dz', \tag{5}$$

where the integration starts at the bottom of the supercell. As a measure of the degree of localization we use the distance w within which $I(z)$ increases from 10 to 90%. We will refer to w as the localization parameter, or simply localization.

In Fig. 5 we display these quantities for SF(42) and SF(24) in $6H$-SiC [for SF(31) and SF(13) in $4H$-SiC, see Ref. 4]. The localization parameters (w_B) are also collected in Table II. The results clearly show that SF's in $4H$- and $6H$-SiC give rise to localized SF bands in which the electron has a strongly enhanced probability to be in the immediate vicinity of the SF plane. Of course, in contrast to the case of localized point defect states, this is only a one-dimensional localization, since an electron in the bound SF state is free to move along the SF plane with an effective mass corresponding to the curvature of the split-off band around the M point.

TABLE III. Valence and conduction band offsets $\Delta E_V(nH/3C)=E_V(nH)-E_V(3C)$ and $\Delta E_C(nH/3C)=E_C(nH)-E_C(3C)$, respectively, for interfaces between three different hexagonal SiC polytypes (n=2, 4, and 6) and $3C$-SiC. The valence band offsets are determined from the calculated value $\Delta E_V(2H/3C)=0.13$ eV (Refs. 19 and 20) and assuming that they are proportional to the degree of hexagonality (100% in $2H$-, 50% in $4H$-, and 33% in $6H$-SiC), as suggested in Ref. 20. The conduction band offsets are obtained using the experimental values (cf., for instance, Table I in Ref. 21) $E_G(3C)=2.4$ eV, $E_G(2H)=3.3$ eV, $E_G(4H)=3.2$ eV, and $E_G(6H)=3.0$ eV. The valence band offsets are in good agreement with those calculated in Ref. 19. By taking appropriate differences, the band edge offsets between the hexagonal polytypes can be estimated, neglecting interface-dependent charge rearrangement effects.

SiC interface	ΔE_V (eV)	ΔE_C (eV)
$2H/3C$	0.13	1.03
$4H/3C$	0.07	0.87
$6H/3C$	0.04	0.64

The question arises what is causing this strong localization. It is well understood that heavily deformed, broken or chemically perturbed bonds around point defects (regarded as a zero-dimensional defect) can give rise to gap states and three-dimensional localization of the wave function. Two-dimensional localization around dislocations (a one-dimensional defect) and one-dimensional localization in the vicinity of surfaces (regarded as a two-dimensional defect) can also be understood in terms of deformed or broken bonds, but requires interaction between individual sites along the dislocation line or surface to account for the lower dimensions of the localization. In the case of SF's, however, strongly perturbed bonds are not involved in an obvious way as for a surface, since the crystal retains its perfect structure (apart from a very small relaxation of the lattice which is irrelevant for this discussion) on either side of the SF plane.

In Ref. 4 it was suggested, without quantitative justification, that the one-dimensional localization arises because the split-off states belong to a quantum-well (QW) formed by the local $3C$-like stacking sequence around the SF (see Fig. 2). This suggestion was based on two facts. (1) The wave functions for the split-off states are well localized and to a large extent contained in the local $3C$-like (straight) stacking sequence. (2) The conduction band minimum in $3C$-SiC is well below the conduction band minimum in $4H$- or $6H$-SiC (see Table III).

To investigate whether this interpretation in terms of a thin QW is at all realistic and possibly lend further support to it, we will now estimate the binding energy and wave function localization using a simple one-dimensional theory for quantum square wells.[22] Since the lattice constant c for $4H$-SiC, for instance, is close to 10 Å, it seems as a reasonable estimate to assume a quantum-well width of 5 Å (or 4 Å to make a sensitivity check) [see Fig. 2] for both SF(31) and SF(13). Assuming a quantum-well depth of 0.87 eV [i.e., the conduction band offset $\Delta E_C(4H/3C)$ from Table III], and the effective mass 0.3 free electron masses (the effective

mass for 3C-SiC in the [111]-direction calculated from the effective mass components in Ref. 23), the quantum-well model results in one bound state with binding energy 0.24 eV (0.18 eV for a 4 Å quantum well), having wave (envelope) function localization $w=6.1$ Å (7.0 Å). In the cases of SF(42) and SF(24) in 6H-SiC, we have used a QW depth of 0.64 eV (Table III and a QW width of 7.0 Å (or 6.0 Å to check the sensitivity), resulting in one bound state with energy 0.22 eV (0.19 eV) below the conduction band minimum, with localization $w\approx 6.5$ Å ($w\approx 7.0$ Å). These results are reproduced in Table II for comparison with the results from the supercell calculations. The approximate agreement suggests that the QW interpretation is indeed realistic, and supports the idea that *the one-dimensional localization can be understood as a quantum-well confinement effect*.

Of course, the simple square shape of the quantum well potential used here to interpret the numerical results is chosen only because of its analytical simplicity. It has been shown both in Ref. 19 and 20 that a 2H/3C interface induces a dipole moment in the vicinity of the interface. We therefore also expect a dipole moment at a 4H/3C (and 6H/3C) interface, since the dipole moment in principle originates from the hexagonal symmetry. The electric field associated with such a dipole moment can change the electrostatic potential, leading to a potential shape that is different from a simple square well. But even though this model is simple and crude, both with respect to the shape, the width, and the depth of the quantum well, we think the arguments above do indeed suggest that SF(31) and SF(13) in 4H-SiC, and SF(42) and SF(24) in 6H-SiC are each associated with a QW of some shape, and that a QW model offers a helpful and reasonable description of the SF results.

B. Cases where the stacking fault acts as a quantum barrier

In Figs. 3 and 4 we saw that SF(3111) and SF(111) do not give rise to clearly split-off states in the fundamental band gap similar to those in the other cases, although in both cases a split-off conduction band appears at the K point, which is the point where 2H-SiC has its conduction band minimum. To analyze the absence of clearly split-off bands in the fundamental band gap in these cases, we first turn to SF(111) in 3C-SiC and observe (Fig. 2) that SF(111) creates a thin 2H-like (zig zag) sequence consisting of two hexagonal turns (i.e., two changes of sign in the Hägg sequence) in neighboring glide planes. From Table III we find that both for the conduction band and the valence band electrons, SF(111) should act as a quantum *barrier* rather than a quantum well, with barrier heights estimated to 1.03 and 0.13 eV, respectively. An electron-repulsive barrier acting on the conduction band electrons is not expected to give rise to bound states below the conduction band. On the other hand, a quantum barrier (as with any other repulsive perturbation) acting on the valence band electrons, could create bound states in the fundamental band gap originating from the valence band. From Table III the barrier height is around 0.13 eV, but the valence electrons will respond to this perturbation in some way, most likely leading to a rearrangement of the electrons relative to the perfect bulk in such a way that the *thin* 2H-like stacking sequence becomes slightly depleted of electronic charge, resulting in a slightly positively charged SF sheet. This will reduce the barrier height to less than 0.13 eV. Our results indicate that the resulting perturbation does not create states clearly split off from the valence band. Below (Sec. IV C) we will see that this perturbation does not even seem to create shallow states in the gap.

The situation for SF(3111) in 6H-SiC is similar (see Fig. 2). In this case, a 2H-like (zig zag) sequence with four hexagonal turns surrounded by locally cubic stacking sequences (two extra turns compared to perfect 6H-SiC) is created. The geometrical resemblance with the SF in 3C-SiC, which has two hexagonal turns, is obvious. Furthermore, assuming that the band offsets in Table III approximately also describe the band edge offsets at a 2H/6H junction, we get $\Delta E_C(2H/6H)=E_C(2H)-E_C(6H)\approx 0.4$ eV and $\Delta E_V(2H/6H)=E_V(2H)-E_V(6H)\approx 0.1$ eV. Thus, both for the conduction band and the valence band electrons, SF(3111) acts as a quantum *barrier*. Thus, there is not only a geometrical resemblance with the SF in 3C-SiC, but also a resemblance with respect to the height of the energy barriers [but with a lower conduction band energy barrier for SF(3111) than for SF(111)].

C. Polarization-induced localization of near band edge states

In Fig. 6(a) we show the projected probability distribution $f_\alpha(z)$ for the bottom of the conduction band ($\alpha=M$) in the case SF(13) (which is very similar to the one for SF(31) shown in Ref. 4) together with $f_\alpha(z)$ for the top of the valence band ($\alpha=\Gamma$) for the cases SF(13) [Fig. 6(b)] and SF(31) [Fig. 6(c)] in 4H-SiC. The striking feature here is that the valence-band-edge probability distribution for SF(13) in Fig. 6(b) has the appearance of a localized state (in one dimension), essentially localized around the SF, but with a localization $w\approx 28$ Å, which is much larger than for the bound SF(13) state at $(E_C-0.18)$ eV, for which $w\approx 8.6$ Å (see also Table II). Furthermore, this localized highest energy (valence) band state lies very close in energy to the extended valence band states, with no clear signs of split-off. No similar localization can be seen at the valence band edge for SF(31). In the remainder of this section we will present some arguments which we believe explain this and related features in the other cases. This explanation is based on the work and ideas presented by Qteish *et al.*[20]

Figures 7(a) and 7(b) show schematically the *macroscopically averaged*[24] crystal potential energy along the c direction for SF(13) and perfect 4H-SiC, respectively. This macroscopic average is defined as an average in slabs orthogonal to the c direction, and corresponds to the usual definition of macroscopic quantities in electrostatics (cf. the macroscopic Maxwell equations). The construction of the figures is essentially based on two ideas, pointed out in Ref. 20. First, all SiC polytypes, except 3C-SiC, have a symmetry where not all four tetrahedral bonds are equivalent. In Fig. 1(a), for instance, the Si-C bonds along the c direction are not related by symmetry to the three bonds almost lying in the glide plane. Thus, charge transfer between the nonequivalent

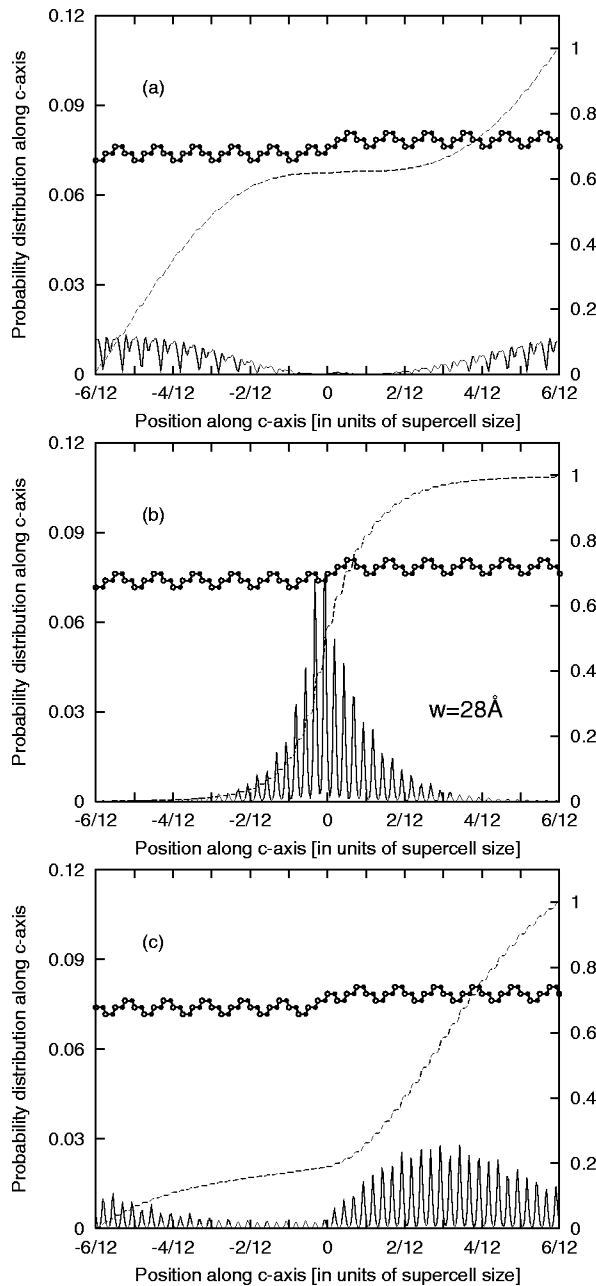

FIG. 6. The projected probability distribution (left-hand scale) and the truncated normalization integral (right-hand scale), within a 96 atom supercell, at the bottom of the conduction band at M for SF(13) (a), and at the top of the valence band at Γ for SF(13) (b), and SF(31) (c) in $4H$-SiC. Also shown are the stacking sequence and the localization w for localized states.

bonds may (and does) take place, resulting in a spontaneous polarization (SP) (cf. ferroelectric or pyroelectric materials) along the c direction. The electric dipole moments associated with the SP are essentially localized around the hexagonal turns in the stacking sequence, and are directed opposite to the c direction (down in Fig. 1). The electric (polarization) field from all the dipoles in a plane orthogonal to the c axis is thus directed along the positive c direction. It is helpful to think of this situation as similar to a pair of closely spaced oppositely charged plates (cf. a parallel-plate capacitor)

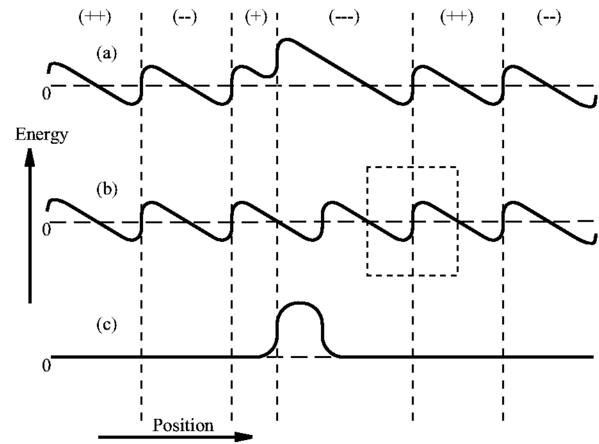

FIG. 7. Schematic illustration of the averaged potential energy along the stacking direction in the case of (a) SF(13), (b) perfect $4H$-SiC, and (c) their difference. The hexagonal c axis is directed to the right, and the rectangular area in (b) indicates half a primitive unit cell.

around each hexagonal turn and parallel with the basal plane, with the negatively charged plate to the right of the positively charged plate in Fig. 7. As is well known, the electric field is zero outside the capacitor, and exists only between the oppositely charged plates. The presence of this electric field is represented in Figs. 7(a) and 7(b) by the positive slopes in the averaged potential energy around the hexagonal turns. In SiC, the energy barrier associated with each dipole is around 0.04 eV. Since a SP does not exist in $3C$-SiC for symmetry reasons, the dipole moment per unit volume is to a good approximation proportional to the degree of hexagonality.

Second, to avoid the build-up of a large uncompensated electric field (voltage) across the crystal, there must exist a *depolarization field* across the crystal, which is directed opposite to the polarization field and compensates for the potential steps associated with the hexagonal turns. Such a depolarization field will arise in a real crystal from the accumulation of surface charges on the material, from the motion of free carriers in the bulk or from the polarization of dopants.[20] In addition, intrinsic screening effects in the perfect crystal will also lead to a depolarization field. All these effects, except for the accumulation of surface charges, give rise to a finite screening length, which is the distance from an electrostatic perturbation beyond which the perturbation is screened out. In Fig. 7 it has been assumed that the screening length is not substantially smaller than the hexagonal lattice constant c in $4H$-SiC, because if it were, the maxima of the potential in Fig. 7(a) would all have essentially the same value. The important point to notice now is that due to the use of a periodic potential, the depolarization field is automatically introduced into the calculations (since the periodic potential has the same value on opposite sides of the supercell), and is represented in Fig. 7 by the portions of the averaged potential having negative slopes between the hexagonal turns.

Figure 7(c) shows the difference between the averaged potentials in Figs. 7(a) and 7(b). It can be regarded as the

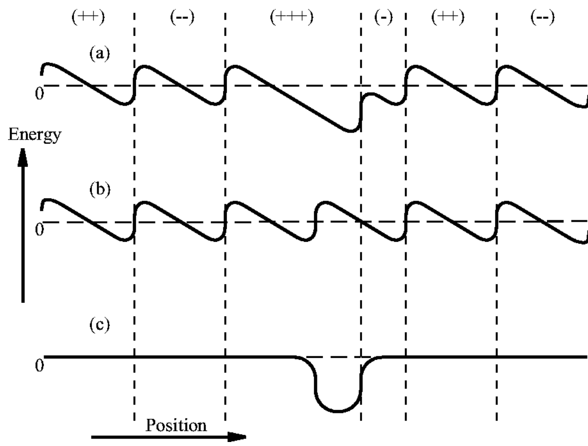

FIG. 8. Same as Fig. 7 but for SF(31).

average of a perturbation acting on the perfect crystal to create a potential in the faulted crystals. Since the averaged perturbation is positive, the perturbation itself, i.e., the difference in potential energy as a function of the three-dimensional position vector $\vec{r}$ between crystals with and without SF(13), can be considered repulsive as a whole. We argue that, in analogy with point defect physics, this repulsive perturbation is capable of creating localized band states just above the top of the (extended) valence band states. Since they are in the gap (but just barely so), they are localized [Fig. 6(b)], just like discrete shallow acceptor states in semiconductors. These localized band states, however, are completely occupied and cannot act as acceptors.

The absence of similar localized band states in the case of SF(31) can be explained within the same conceptual framework. The averaged potentials in this case are shown in Figs. 8(a) and 8(b), and as seen in Fig. 8(c), their difference is negative, corresponding now instead to an attractive perturbation. Such a perturbation will not push up states from the valence band and into the band gap, but the highest-energy valence band state should essentially be modified host crystal band state [Fig. 6(c)]. Note that the relative energy positions of the strongly localized sates at $E_C-0.22$ eV and $E_C-0.18$ eV is, at least qualitatively, compatible with the difference between the potentials in Figs. 8 and 7, and can probably be traced back to this difference. Moreover, the difference in sign between the two perturbation potentials in Figs. 7(c) and 8(c) is a manifestation and another proof of the inequivalence of the two types of SF's, SF(31), and SF(13). This inequivalence has to our knowledge not been recognized in the literature before, even though it can be inferred from general symmetry considerations alone (Sec. II A).

The projected probability distributions for the lowest conduction band state and highest valence band state for SF(111) in 3*C*-SiC are shown in Figs. 9(a) and 9(b). Again, even though they are very close in energy to the delocalized band states in their respective bands, they are also surprisingly localized, in particular the valence band state with localization $w\approx 18$ Å. We also observe that they have most of their wave functions in the 3*C* host region outside the thin 2*H*-like stacking sequence, and, which is perhaps more mysterious, with amplitudes almost exclusively on *different sides*

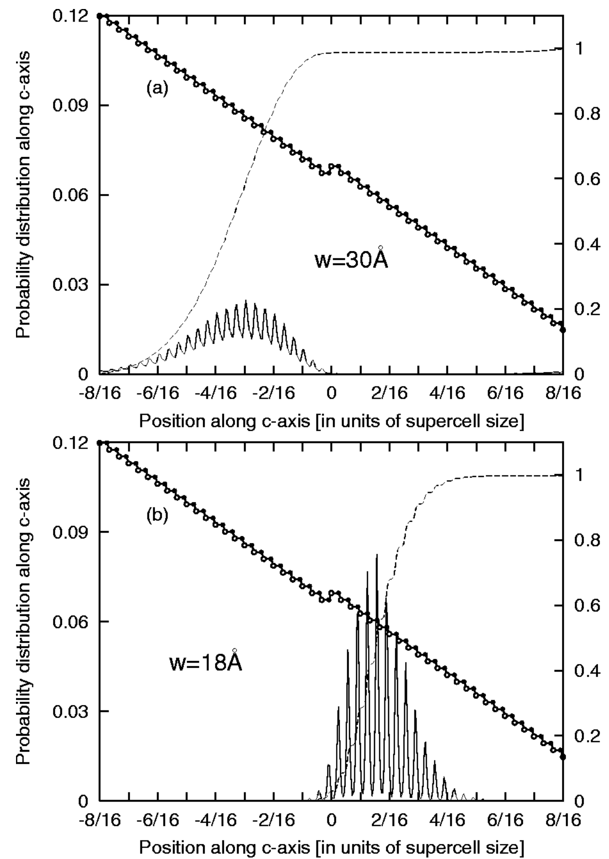

FIG. 9. The projected probability distribution (left-hand scale) and the truncated normalization integral (right-hand side), within a 96 atom supercell, for (a) the bottom of the conduction band and (b) the top of the valence band in 3*C*-SiC with a SF.

of the SF. Next we will explain these features, and again we will consider the effects of SP and the associated depolarization field.[20]

First we observe that a distinct difference between the SF in 3*C*-SiC and those in 4*H*-SiC is that in the former case two *extra* hexagonal turns are introduced relative to the host crystal, whereas in the latter case only the *position* of one hexagonal turn has changed, without changing the total number of turns. The conservation of the number of hexagonal turns is the reason why the averaged perturbation for the SF's in 4*H*-SiC is localized (the perturbation itself exists, of course, in the whole displaced part of the crystal). In contrast, the averaged perturbation for a SF in 3*C*-SiC (as well as for SF(3111) in 6*H*-SiC, see below) will, except for details around the hexagonal turns, schematically look similar to that in Fig. 10. Again the portion with the positive slope is due to the dipole moment associated with the hexagonal turns (here indicated by one structureless step), and the portions with the negative slopes on either side are associated with the depolarization field. We believe that it is this shape of the perturbation which is responsible for the wave function segregation: on the right-hand side of the extra hexagonal turns the repulsive perturbation pushes up a state from the valence band and into the gap, making it localized, while on the other side the attractive part creates a localized state just below the conduction band. Thus, it is not the thin va-

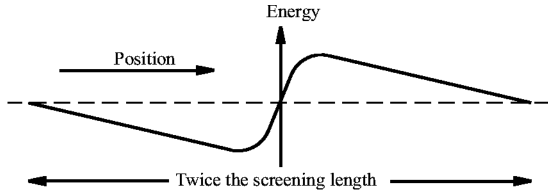

FIG. 10. Schematic illustration of the averaged potential along the c axis inside a $3C$-SiC supercell caused by the introduction of one or several additional hexagonal turns in neighboring (0001) planes. For simplicity, the potential associated with the dipole moment is indicated with one structureless step. The figure is also applicable to SF(3111) if regarded as a plot of the averaged potential perturbation.

lence electron quantum barrier (of height less than 0.13 eV in this case) in itself which creates these states close to the band edges, but rather the presence of the polarization in the thin $2H$-like slab and the accompanying depolarization field. This interpretation is supported by our calculations on so-called twin boundaries in $3C$-SiC,[25] which is a $3C$ crystal containing one hexagonal turn. In this case we observe a wave function segregation and localization for the states at the band edges which is almost identical to that in SF(111). It should be noted that these conclusions are of general validity only if twice the screening length is not much larger than the length of the supercell in the c direction, since otherwise the slope of the potential from the depolarization field in Fig. 10 is affected by the size of the supercell.

Based on the results for $4H$- and $3C$-SiC, the appearance of localized states at the immediate vicinity of the band edges for SF's in $6H$-SiC can easily be understood. In Fig. 11 we show $f_{\alpha}(z)$ for the bottom of the conduction band ($\alpha=M$) in the case SF(24) [which is very similar to that for SF(42)], together with $f_{\alpha}(z)$ for the top of the valence band ($\alpha=\Gamma$) for the case SF(24) and SF(42). From Fig. 2 it is clear that the situation for SF(24) corresponds to Fig. 7, thus creating similar to SF(13) in $4H$-SiC, localized band states just above the extended band states at the valence band maximum [Fig. 11(b)]. Similarly, SF(42) behaves as SF(31) in $4H$-SiC in this respect, while SF(3111) introduces two extra hexagonal turns relative to the host crystal, very similar to SF(111) in $3C$-SiC. This resemblance between SF(3111) in $6H$-SiC and SF(111) in $3C$-SiC is reflected in Fig. 12, which is very similar to Fig. 9.

The absence and presence, respectively, of a shallow localized state close to the valence band in the case SF(42) and SF(24) indicate that there is a difference in their optical activity. If ψ_i denotes the wave function for the strongly localized state below the conduction band minimum and ψ_f the wave function for the highest state on the other side of the band gap, the probability for an optical transition across the band gap is proportional to $|\langle \psi_i|\vec{r}|\psi_f\rangle|^2$. Figures 5 and 11 clearly indicate that this transition probability is much larger for SF(24) than for SF(42) in $6H$-SiC. The corresponding difference between SF(13) and SF(31) in $4H$-SiC is similar. The localization parameters for the localized near band-edge states are summarized in Table II.

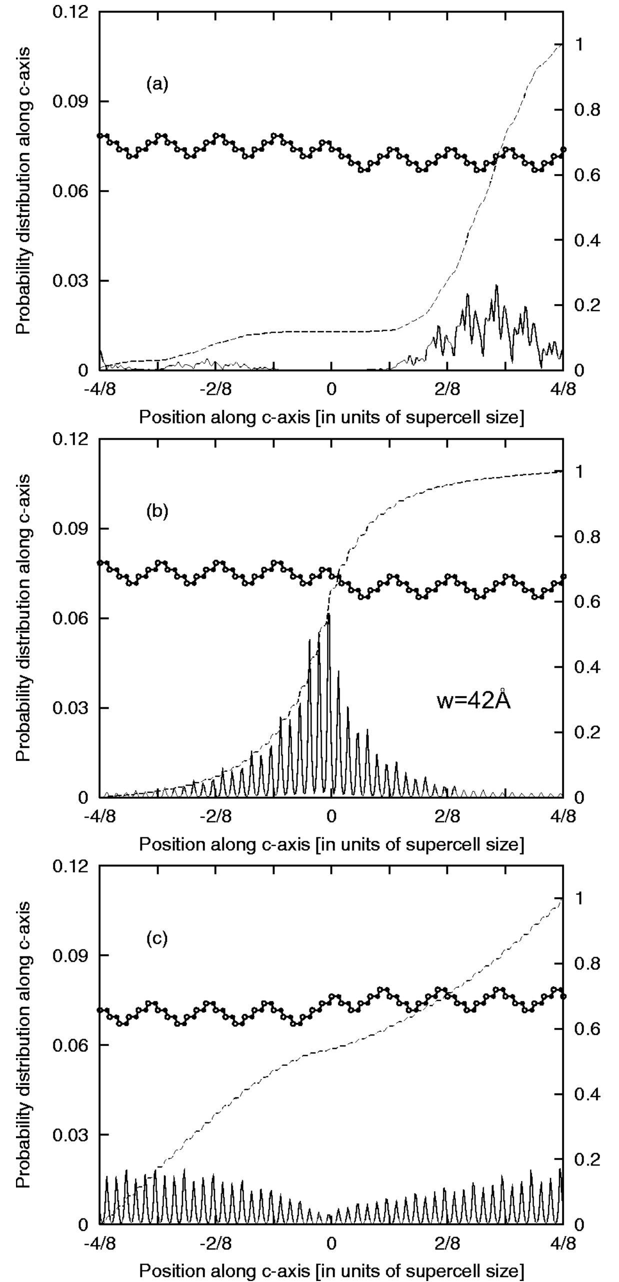

FIG. 11. The projected probability distribution (left-hand scale) and the truncated normalization integral (right-hand scale), within a 96 atom supercell, at the bottom of the conduction band at M for SF(24) (a), and at the top of the valence band at Γ for SF(24) (b) and SF(42) (c) in $6H$-SiC. Also shown are the stacking sequence and the localization w for localized states.

V. SOME EXPERIMENTAL OBSERVATIONS EXPLAINED BY SF FORMATION

In Ref. 4 we showed how an observed resistivity anomaly in n-type $4H$- and $6H$- SiC,[26] which cannot be reconciled with the normal bulk anisotropy,[27,28] could be explained in terms of the strongly localized SF bands. We also briefly indicated their relation to the electrical degradation phenomenon in bipolar devices. Here we will be a little more detailed regarding the mechanism leading to degradation.

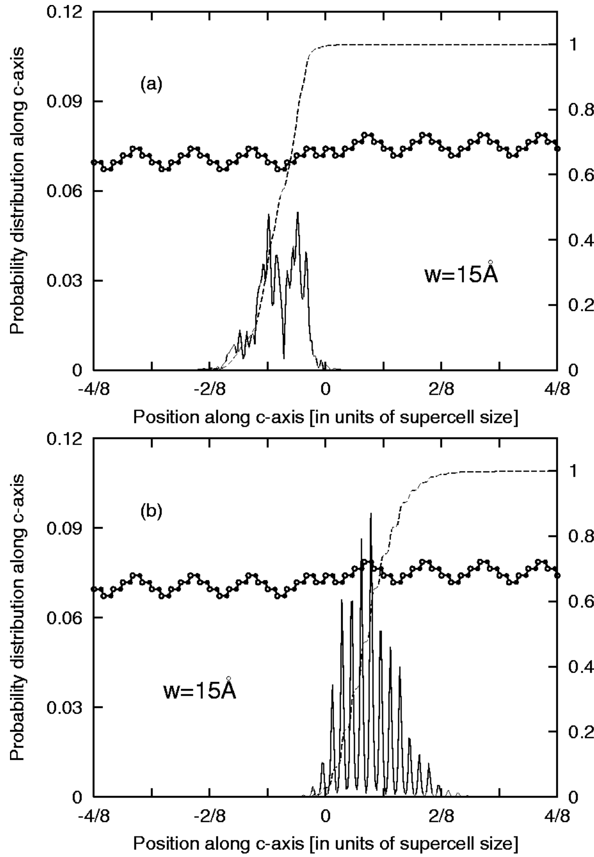

FIG. 12. The projected probability distribution (left-hand scale) and the truncated normalization integral (right-hand scale), within a 96 atom supercell, for (a) the bottom of the conduction band and (b) the top of the valence band in 6H-SiC containing SF(3111).

Even though there are shallow states in the immediate vicinity of the band edges which show clear signs of localization, we argue that the bound SF states in the clearly split-off band in Table II are mainly responsible for the degradation of bipolar 4H- and 6H-SiC devices. Electrons injected into the base region of the pin diode, for instance, are captured by the bound SF states, tending to make this SF negatively charged, whereby holes are also attracted to the SF region. This enhanced local concentration of electrons and holes will increase the probability for electron-hole recombination, leading to a reduction of the electron and hole lifetimes, and hinder electrons and holes from moving freely in the device. This will obstruct the normal build-up of an electron-hole plasma, and consequently obstruct the normal conductivity modulation, causing an increased voltage drop across the device.

An interesting question is what is causing the expansion of the SF's. This is not the subject of the present paper, but it could be noticed that apart from stress, which is generally too low to cause partial dislocation motion around room temperature in SiC, recombination enhanced dislocation motion[29] is most likely involved.

VI. STACKING FAULT ENERGIES

In crystals where the SF energy is large, perfect dislocations tend not to split up into partial dislocations to any appreciable extent, since the effective pulling force acting on the trailing partial from the leading partial, given by γ/b where b is the length of the Burgers vector, is large. The existence of SF ribbons in SiC, i.e., the area between the leading and the trailing partial, and thus the development of extended SF's, is a manifestation of the small SF energies in that material. For instance, the SF energy in 6H-SiC is around 3 mJ/m^2 and around 15 mJ/m^2 in 4H-SiC,[9,10] compared to 280 mJ/m^2 in diamond,[30] 55 mJ/m^2 in Si, and 45 mJ/m^2 in GaAs (see Ref. 9).

TABLE IV. Theoretical and experimental SF energies (mJ/m^2) for three SiC polytypes. ISR means intrasupercell relaxation, and is defined in the main text.

SF energies (mJ/m^2)		3C-SiC	4H-SiC	6H-SiC
Supercell method	SF I	−1.71	17.7	3.10
(without ISR)	SF II		18.1	40.1
	SF III			3.35
Supercell method	SF I	−2.70	18.4	1.35
(with ISR)	SF II		18.7	38.4
	SF III			1.63
ANNNI model	SF I	−6.27	18.3	3.14
	SF II		18.3	36.6
	SF III			3.14
Experiment	Ref. 9		14.7±2.5	2.9±0.6
	Ref. 10			2.5±0.9

The SF energies of SiC calculated in the present work are shown in Table IV, together with experimental results. In the first-principles supercell method we have calculated the SF energies both with and without intrasupercell relaxation. The meaning of ''without intrasupercell relaxation'' in Table IV is that in neither the perfect crystal nor the faulted crystal have the atoms been allowed to deviate from their ideal positions determined by a and c, whereas ''with intrasupercell relaxation'' means that the atomic positions for both the perfect and the faulted crystals are fully relaxed (for given a and c). From Table IV we see that the effect of intrasupercell relaxation is less than 2 mJ/m^2.

The values for the ANNNI model are based on the following interlayer interaction parameters obtained using Eq. (3) (in meV): $J_1=1.9097$, $J_2=-2.3059$, $J_3=-0.3959$, and from these parameters one can determine the approximate SF energies for the other polytypes.[31] As seen in Table IV, the supercell method and the ANNNI model give very similar results, except for 3C-SiC. Note that the ANNNI model cannot distinguish between SF(31) and SF(13), or between SF

TABLE V. Theoretical and experimental SF energies (mJ/m^2) for Si and diamond.

mJ/m^2	Without ISR	With ISR	Experiment
Si	36.0	33.4	50–70 (Ref. 33)
C (diamond)	314	264	279±41 (Ref. 30)

(42) and SF(24), since it only concerns normal and twinned tetrahedra, whereas SF(31) and SF(13), as well as SF(42) and SF(24), are related through an interchange of Si and C atoms. The SF energy of $3C$-SiC is negative both with the supercell method and from the ANNNI model, which is in agreement with theoretical results obtained earlier by Käckel *et al.*[32]

In order to investigate the accuracy of our computational method, we have also calculated the SF energy in Si and diamond including intrasupercell relaxation (Table V). The theoretical SF energy of diamond agrees very well with experimental values, while for Si it is clearly smaller than the available experimental value. Chou *et al.*[33] and Käckel *et al.*[32] also calculated the SF energy of Si and obtained values close of ours, namely 33 and 38 mJ/m^2, respectively. We have not been able to find the reasons for the apparent underestimations of the SF energy for Si relative to experiments.

A striking feature in Table IV is that in $6H$-SiC, SF(3111) has a considerably larger SF energy than the other two types. Unless there is a preference as to in which glide plane partial dislocations are nucleated, this type of SF should be relatively rare compared to the other two types.

ACKNOWLEDGMENTS

The authors gratefully acknowledge financial support from the Swedish Foundation for Strategic Research (SSF), the Swedish Research Council (VR), and the National Supercomputer Center (NSC) in Sweden for computer time.

---

[1] J. P. Bergman, H. Lendenmann, P. Å. Nilsson, U. Lindefelt, and P. Skytt, Mater. Sci. Forum **353-356**, 299 (2000).
[2] A. Galeckas, J. Linnros, B. Breitholtz, and H. Bleichner, J. Appl. Phys. **90**, 980 (2000).
[3] J. Q. Liu, M. Skowronski, C. Hallin, R. Söderholm, and H. Lendenmann, Appl. Phys. Lett. **80**, 749 (2002).
[4] H. Iwata, U. Lindefelt, S. Öberg, and P. R. Briddon, Phys. Rev. B **65**, 033203 (2002); Mater. Sci. Forum **389-393**, 529 (2002).
[5] M. S. Miao, S. Limpijumnong, and W. Lambrecht, Appl. Phys. Lett. **79**, 4360 (2001).
[6] S. G. Sridhara, F. H. C. Carlsson, J. P. Bergman, and E. Janzén, Appl. Phys. Lett. **79**, 3944 (2001).
[7] J. P. Bergman, H. Jakobsson, L. Storasta, F. H. C. Carlsson, B. Magnusson, S. Sridhara, G. Pozina, H. Lendenmann, and E. Janzén, Mater. Sci. Forum **389-393**, 9 (2002).
[8] C. Cheng, R. J. Needs, and V. Heine, J. Phys. C **21**, 1049 (1988).
[9] M. H. Hong, A. V. Samant, and P. Pirouz, Philos. Mag. A **80**, 919 (2000).
[10] K. Maeda, K. Suzuki, S. Fujita, M. Ichihara, and S. Hyodo, Philos. Mag. A **57**, 573 (1988).
[11] D. Hull and D. J. Bacon, in *Introduction to Dislocations*, 3rd ed. (Butterworth-Heinemann, London, 1984).
[12] In Ref. 4 we used a different order for the SF's in $6H$-SiC, namely (in the notation previous→present) SF I→SF III, SF II→SF I, SF III→SF II.
[13] P. R. Briddon, EIMS Data Rev. **20**, 330 (1999); J. Coutinho, R. Jones, P. R. Briddon, and S. Öberg, Phys. Rev. B **62**, 10 824 (2000).
[14] N. Troullier and J. L. Martins, Phys. Rev. B **43**, 1993 (1991).
[15] G. B. Bachelet, D. R. Hamann, and M. Schlüter, Phys. Rev. B **26**, 4199 (1982).
[16] H. J. Monkhorst and J. D. Pack, Phys. Rev. B **13**, 5188 (1976).
[17] *Properties of Silicon Carbide*, edited by G. L. Harriss, EMIS Datareviews Series No. 13 (Institution of Electrical Engineers, London, 1995).
[18] A. Bauer, J. Kräusslich, L. Dressler, P. Kuschnerus, J. Wolf, K. Goetz, P. Käckel, J. Furthmüller, and F. Bechstedt, Phys. Rev. B **57**, 2647 (1998).
[19] F. Bechstedt, P. Käckel, A. Zywietz, K. Karch, B. Adolph, K. Tenelsen, and J. Furthmüller, Phys. Status Solidi B **202**, 35 (1997); F. Bechstedt and P. Käckel, Phys. Rev. Lett. **75**, 2180 (1995).
[20] A. Qteish, V. Heine, and R. J. Needs, Phys. Rev. B **45**, 6534 (1992); *ibid.* **45**, 6376 (1992).
[21] W. van Haeringen, P. A. Bobbert, and W. H. Backes, Phys. Status Solidi B **202**, 63 (1997).
[22] G. Bastard, in *Wave Mechanics Applied to Semiconductor Heterostructures*, Monographies de Physique (Les Editions de Physique, Les Ulis, France, 1992).
[23] C. Persson and U. Lindefelt, J. Appl. Phys. **82**, 5496 (1997).
[24] A. Baldereschi, S. Baroni, and R. Resta, Phys. Rev. Lett. **61**, 734 (1988).
[25] H. Iwata, U. Lindefelt, S. Öberg, and P. R. Briddon, to appear in Mater. Sci. Forum.
[26] J. Takahashi, N. Ohtani, M. Katsuno, and S. Shinoyama, J. Cryst. Growth **181**, 229 (1997); Mater. Sci. Forum **264-268**, 25 (1998).
[27] M. Schadt, G. Pensl, R. P. Devaty, W. J. Choyke, R. Stein, and D. Stephani, Appl. Phys. Lett. **65**, 3120 (1994).
[28] H. Iwata, K. M. Itoh, and G. Pensl, J. Appl. Phys. **88**, 1956 (2000); H. Iwata and K. M. Itoh, *ibid.* **89**, 6228 (2001).
[29] K. Maeda and S. Takeuchi, in *Dislocations in Solids*, edited by F. R. N. Nabarro and M. S. Duesbury (North-Holland Publishing, Amsterdam, 1996), Chap. 10.
[30] P. Pirouz, D. J. H. Cockayne, N. S. Sumida, P. Hirsch, and A. R. Lang, Proc. R. Soc. London, Ser. A **386**, 241 (1983).
[31] H. Iwata, U. Lindefelt, S. Öberg, and P. R. Briddon, Mater. Sci. Forum **389-393**, 439 (2002).
[32] P. Käckel, J. Furthmüller, and F. Bechstedt, Phys. Rev. B **58**, 1326 (1998).
[33] M. Y. Chou, M. L. Cohen, and S. G. Louie, Phys. Rev. B **32**, 7979 (1985).